Supporting Material for
Multi-scale, radially anisotropic shear wave imaging of the mantle underneath the contiguous United States through joint inversion of USArray and global datasets
by Porritt, Becker, Boschi, and Auer

Manuscript in press at Geophysical Journal International, May 2021

This file provides supplementary supporting material to the main text. In particular, we provide:

1. Table S1, listing all of the data types used in our inversion for the new SAVANI-US tomographic model. This is expanded from Table 1 in the main text which only lists the new data.
2. Figure S1, which is a plot of the data adaptive mesh at each model depth.
3. Figure S2, an example trade-off test for evaluation of the roughness damping.
4. Figure S3, a comparison of the isotropic and anisotropic structure as we change the weight of the difference damping.
5. Figure S4, the power spectrum as a function of depth and spherical harmonic degree for the four tomographic models shown in Figure 4 of the main text.
6. Figure S5, map view figures of radial anisotropy focused on the continuous US.
7. Figure S6, a synthetic resolution test with a slab and craton model embedded into SAVANI-US to explore depth resolution.
8. Figures S7 and S8, a comparison of tomographic models for two profiles underneath the continuous US.

Table S1: Full summary of the dataset used in the inversion for SAVANI-US.

Source	Phase	SW mode	SW Period	Number of raypaths	Sensitivity	Weight	Station Distribution
Array Network Facility (ANF)	S	N/A	N/A	220,313	dVsh	15	Contiguous US + Alaska
	SKS	N/A	N/A	12,174	dVsv	9	Contiguous US + Alaska
Lai et al., 2018	ScS	N/A	N/A	23,301	dVsh	3	Global
	ScSScS	N/A	N/A	10,274	dVsh	3	Global
	S	N/A	N/A	129,895	dVsh	15	Global
	SS	N/A	N/A	53,127	dVsh	3	Global
	SSS	N/A	N/A	11,836	dVsh	3	Global

Ekstrom, 2014, 2017	Rayleigh	Fundamental	15	34,504	dVsv	2	Contiguous US
			20	47,620	dVsv	2	Contiguous US
			25	70,914	dVsv	2	Contiguous US
			30	97,199	dVsv	2	Contiguous US
			35	90,712	dVsv	2	Contiguous US
			40	80,844	dVsv	2	Contiguous US
	Love	Fundamental	15	33,233	dVsh	3	Contiguous US
			20	38,407	dVsh	3	Contiguous US
			25	50,239	dVsh	3	Contiguous US
			30	58,955	dVsh	3	Contiguous US
			35	51,474	dVsh	3	Contiguous US
			40	42,160	dVsh	3	Contiguous US
Ritsema et al., 2011	ScS	N/A	N/A	6,449	dVsh	3	Global
	ScSScS	N/A	N/A	11,045	dVsh	3	Global
	ScSScSScS	N/A	N/A	6,941	dVsh	3	Global
	S	N/A	N/A	109,332	dVsh	15	Global
	SKKS	N/A	N/A	7,103	dVsv	9	Global
	SKS	N/A	N/A	25,256	dVsv	9	Global
	sScS	N/A	N/A	1,337	dVsh	3	Global
	sScSScS	N/A	N/A	2,933	dVsh	3	Global
	sScSScSScS	N/A	N/A	2,383	dVsh	3	Global
	sS	N/A	N/A	14,558	dVsh	3	Global
	sSKS	N/A	N/A	2,142	dVsv	9	Global
	SSS	N/A	N/A	20,377	dVsh	3	Glboal
	sSSS	N/A	N/A	2,400	dVsh	3	Global
Ekstrom, 2011	Rayleigh	Fundamental	25	45,316	dVsv	2	Global
			27	45,663	dVsv	2	Global

			30	46,005	dVsv	2	Global
			32	71,639	dVsv	2	Global
			35	71,742	dVsv	2	Global
			40	71,827	dVsv	2	Global
			45	71,886	dVsv	2	Global
			50	100,350	dVsv	2	Global
			60	101,048	dVsv	2	Global
			75	101,085	dVsv	2	Global
			100	100,428	dVsv	2	Global
			125	90,439	dVsv	2	Global
			150	23,217	dVsv	2	Global
			200	23,059	dVsv	2	Global
			250	22,090	dVsv	2	Global
	Love	Fundamental	25	9,698	dVsh	3	Global
			27	9,833	dVsh	3	Global
			30	9,889	dVsh	3	Global
			32	17,373	dVsh	3	Global
			35	17,395	dVsh	3	Global
			40	17,416	dVsh	3	Global
			45	17,441	dVsh	3	Global
			50	38,413	dVsh	3	Global
			60	39,491	dVsh	3	Global
			75	39,527	dVsh	3	Global
			100	38,909	dVsh	3	Global
			125	31,520	dVsh	3	Global
			150	16,332	dVsh	3	Global
			200	14,868	dVsh	3	Global
			250	13,843	dVsh	3	Global
Visser et al., 2008	Rayleigh	Fundamental	35	28,931	dVsv	2	Global
			37	28,931	dVsv	2	Global
			40	28,931	dVsv	2	Global
			43	28,931	dVsv	2	Global
			51	28,931	dVsv	2	Global
			56	28,931	dVsv	2	Global
			62	28,931	dVsv	2	Global
			69	28,931	dVsv	2	Global
			75	28,931	dVsv	2	Global
			88	28,931	dVsv	2	Global
			100	28,931	dVsv	2	Global
			114	28,931	dVsv	2	Global
			125	28,931	dVsv	2	Global

			150	28,931	dVsv	2	Global
			175	28,931	dVsv	2	Global
	Love	Fundamental	35	24,281	dVsh	3	Global
			37	24,281	dVsh	3	Global
			40	24,281	dVsh	3	Global
			43	24,281	dVsh	3	Global
			51	24,281	dVsh	3	Global
			56	24,281	dVsh	3	Global
			62	24,281	dVsh	3	Global
			69	24,281	dVsh	3	Global
			75	24,281	dVsh	3	Global
			88	24,281	dVsh	3	Global
			100	24,281	dVsh	3	Global
			114	24,281	dVsh	3	Global
			125	24,281	dVsh	3	Global
			150	24,281	dVsh	3	Global
			175	24,281	dVsh	3	Global
	Rayleigh	1st overtone	35	23,995	dVsv	1	Global
			37	23,995	dVsv	1	Global
			40	23,995	dVsv	1	Global
			43	23,995	dVsv	1	Global
			46	23,995	dVsv	1	Global
			50	23,995	dVsv	1	Global
			56	23,995	dVsv	1	Global
			61	23,995	dVsv	1	Global
			69	23,995	dVsv	1	Global
			77	23,995	dVsv	1	Global
			87	23,995	dVsv	1	Global
			99	23,995	dVsv	1	Global
			113	23,995	dVsv	1	Global
			129	23,995	dVsv	1	Global
			148	23,995	dVsv	1	Global
			172	23,995	dVsv	1	Global
	Love	1st overtone	35	20,113	dVsh	1	Global
			37	20,113	dVsh	1	Global
			40	20,113	dVsh	1	Global
			43	20,113	dVsh	1	Global
			46	20,113	dVsh	1	Global
			51	20,113	dVsh	1	Global
			56	20,113	dVsh	1	Global
			62	20,113	dVsh	1	Global
			69	20,113	dVsh	1	Global

			78	20,113	dVsh	1	Global
			88	20,113	dVsh	1	Global
			100	20,113	dVsh	1	Global
			114	20,113	dVsh	1	Global
			131	20,113	dVsh	1	Global
			153	20,113	dVsh	1	Global
			176	20,113	dVsh	1	Global

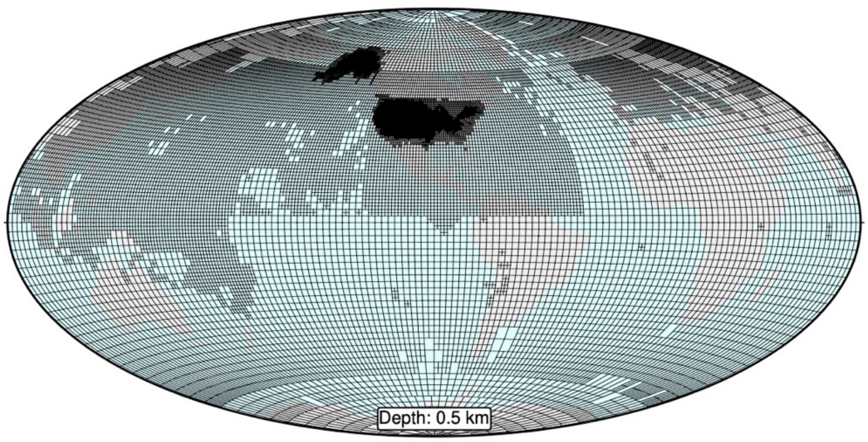

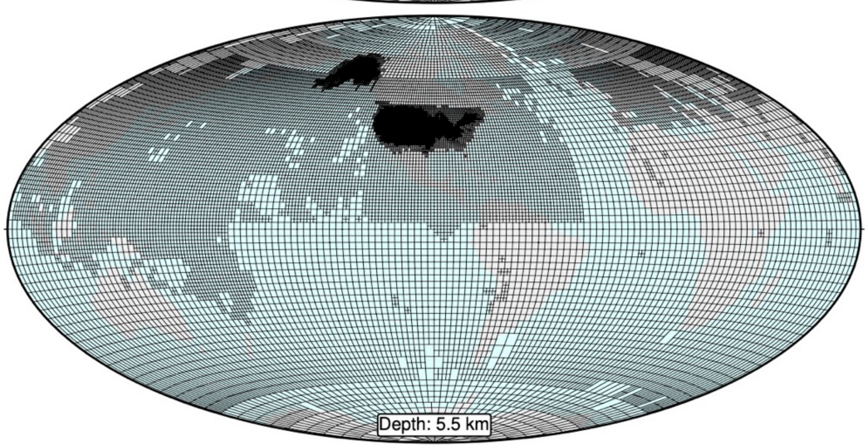

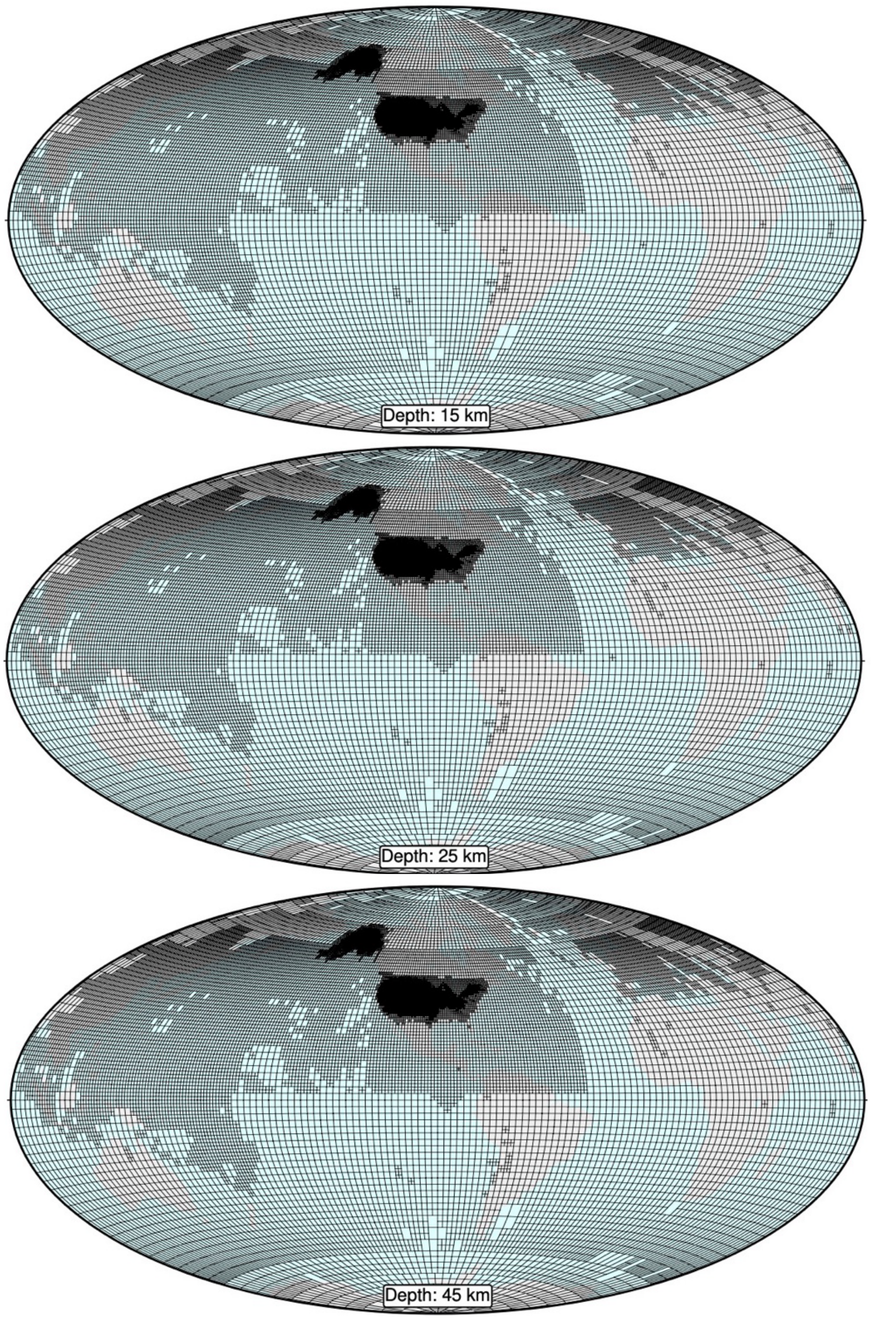
Depth: 15 km
Depth: 25 km
Depth: 45 km

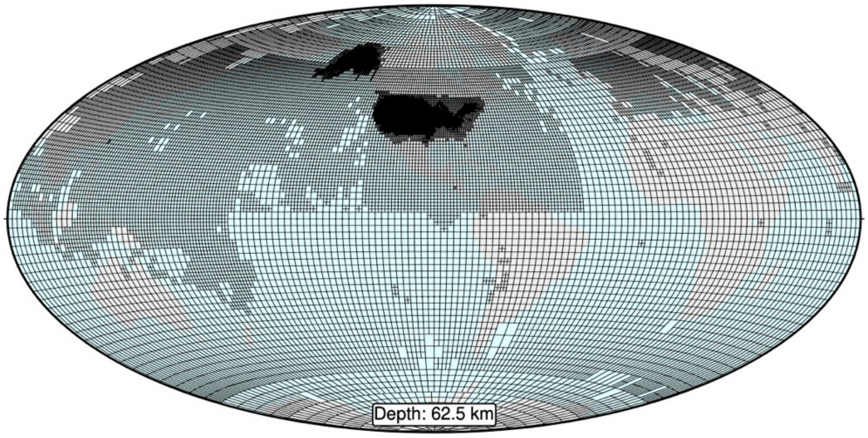
Depth: 62.5 km

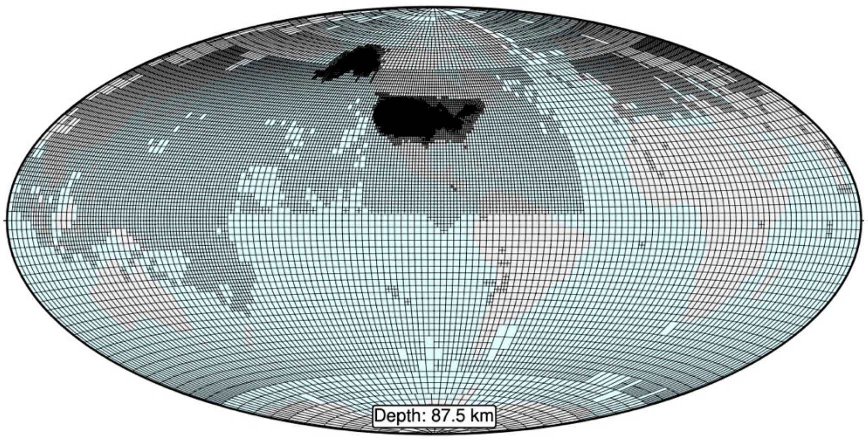
Depth: 87.5 km

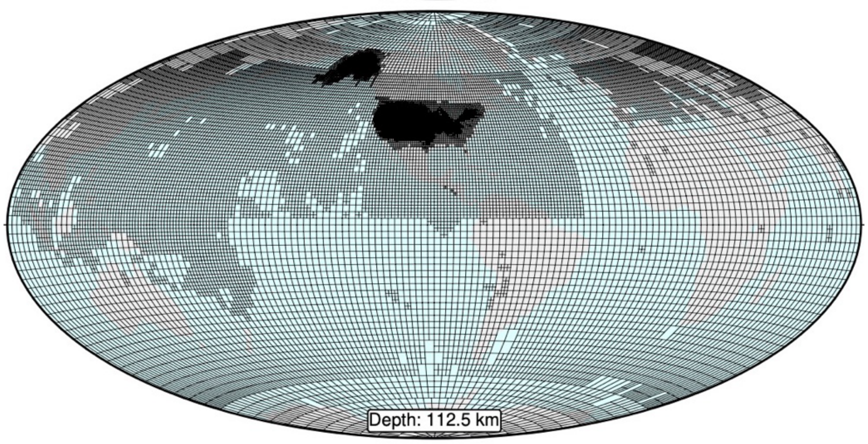
Depth: 112.5 km

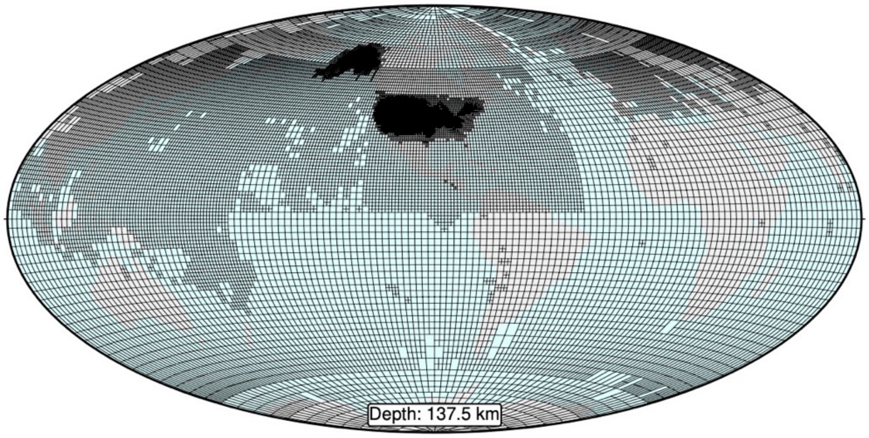
Depth: 137.5 km

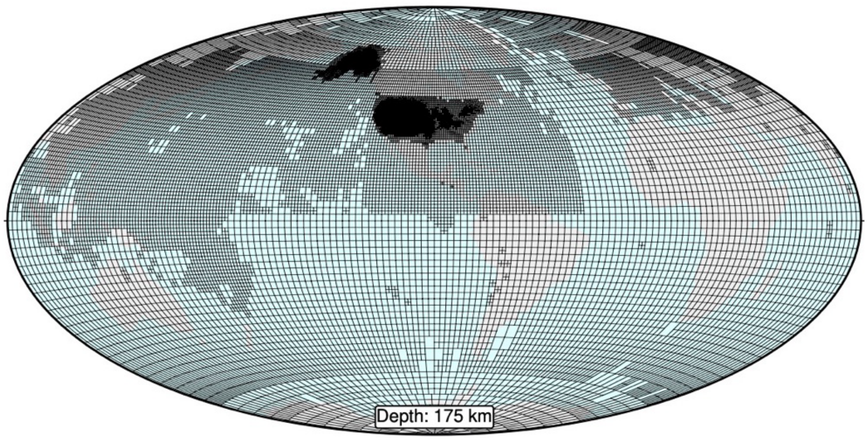
Depth: 175 km

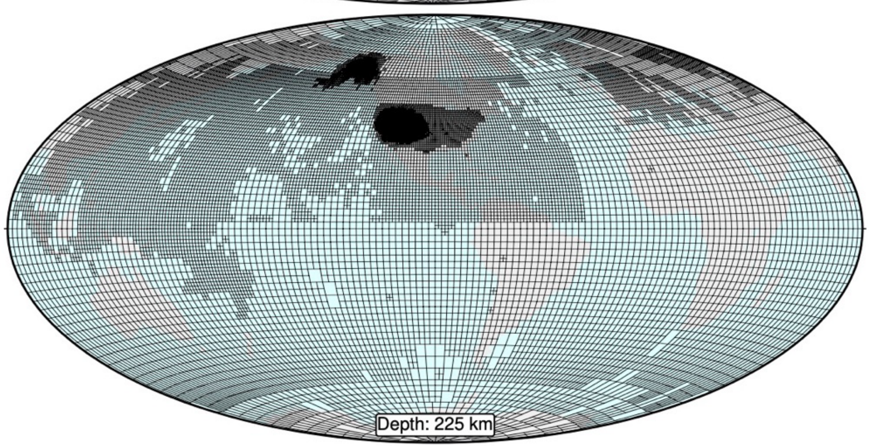
Depth: 225 km

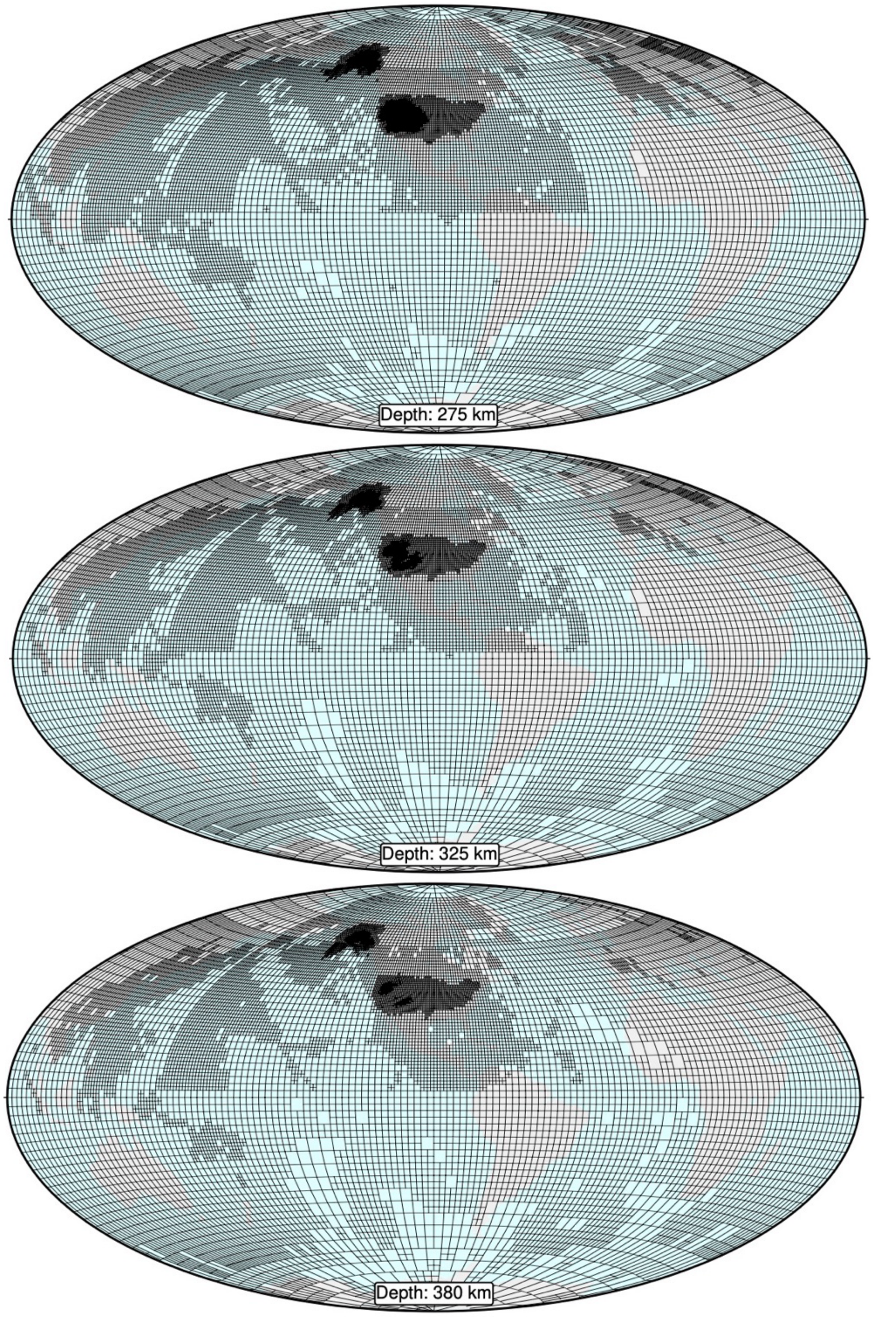
Depth: 275 km
Depth: 325 km
Depth: 380 km

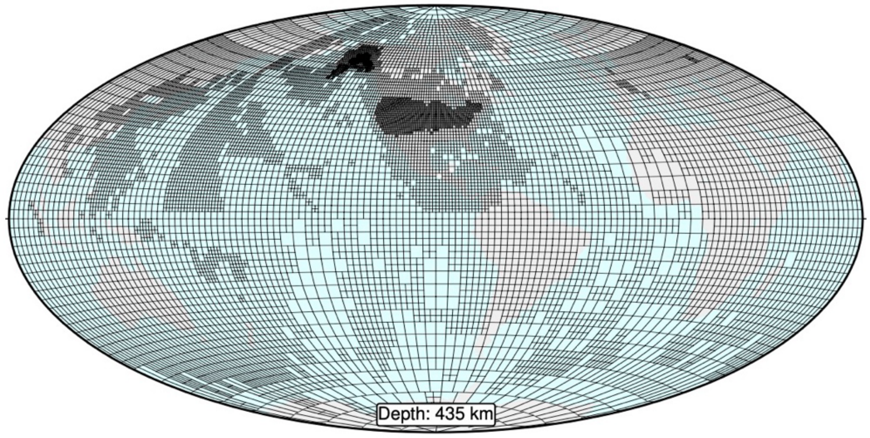
Depth: 435 km

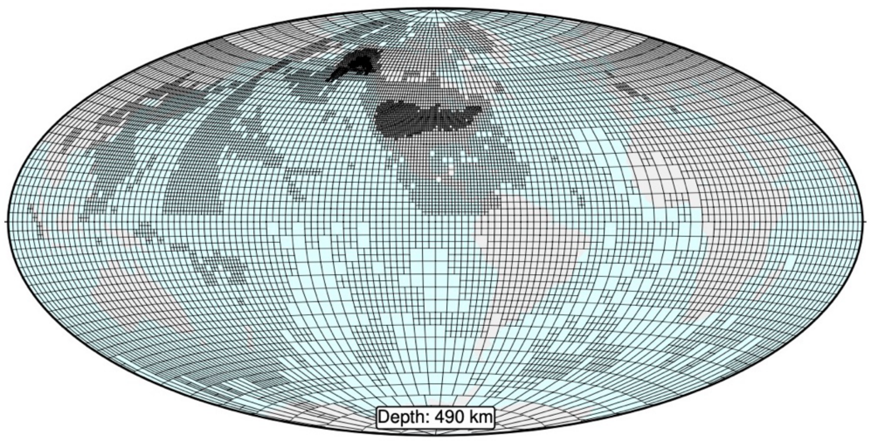
Depth: 490 km

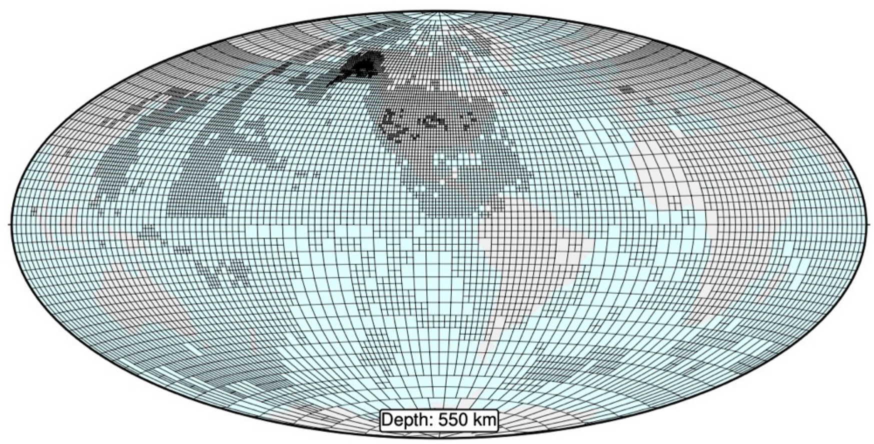
Depth: 550 km

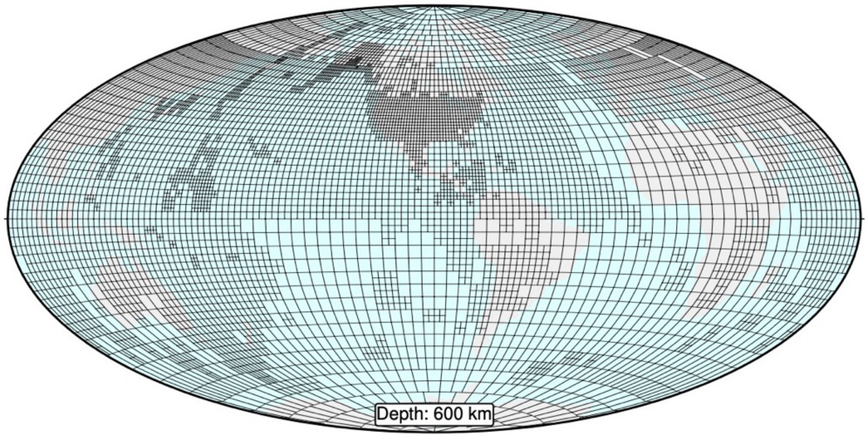
Depth: 600 km

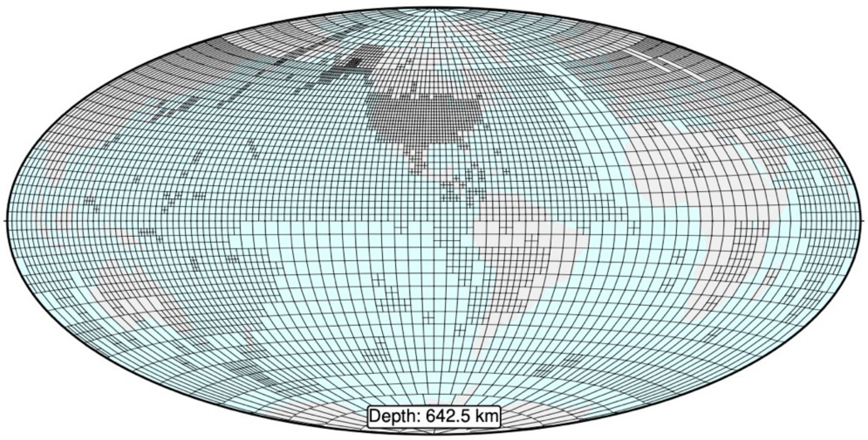
Depth: 642.5 km

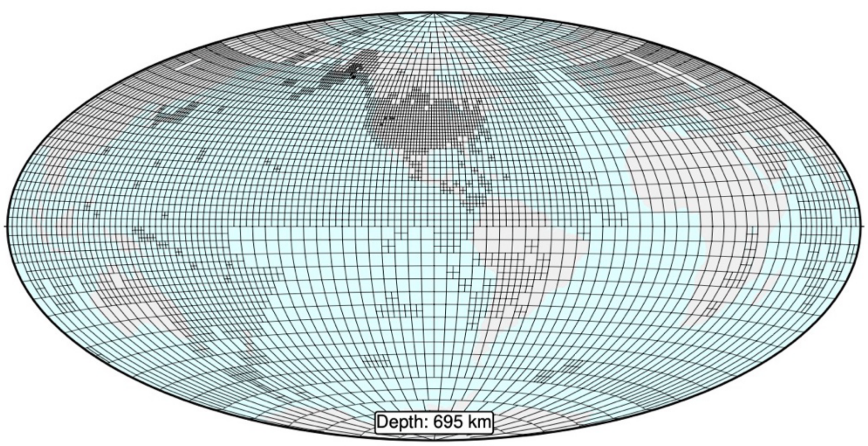
Depth: 695 km

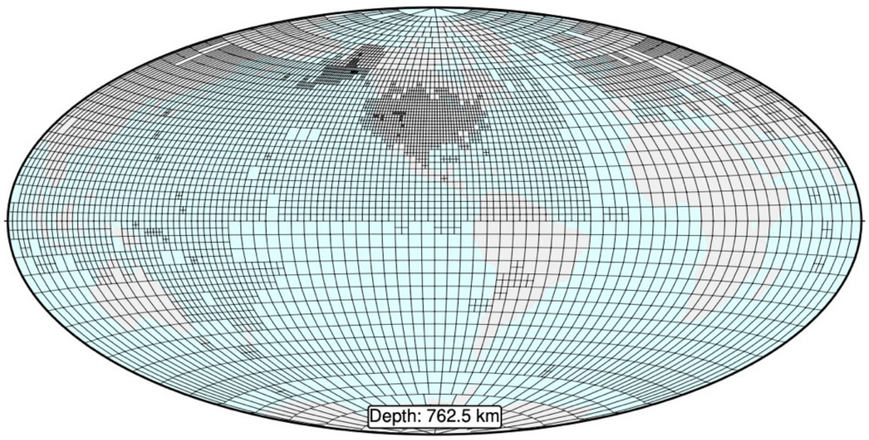
Depth: 762.5 km

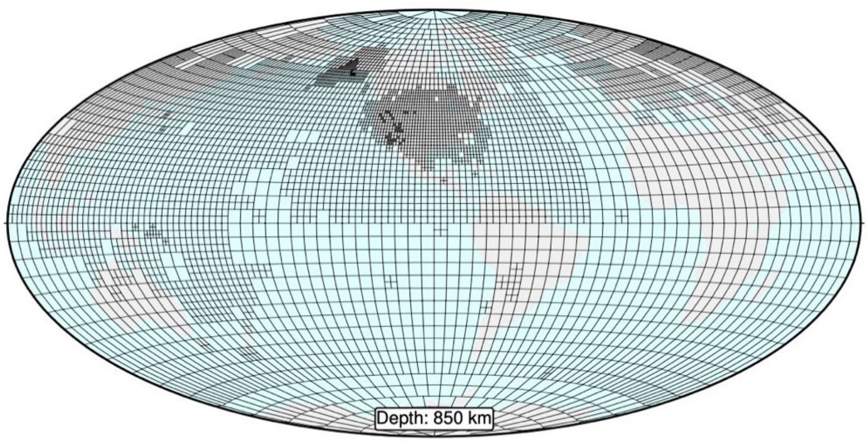
Depth: 850 km

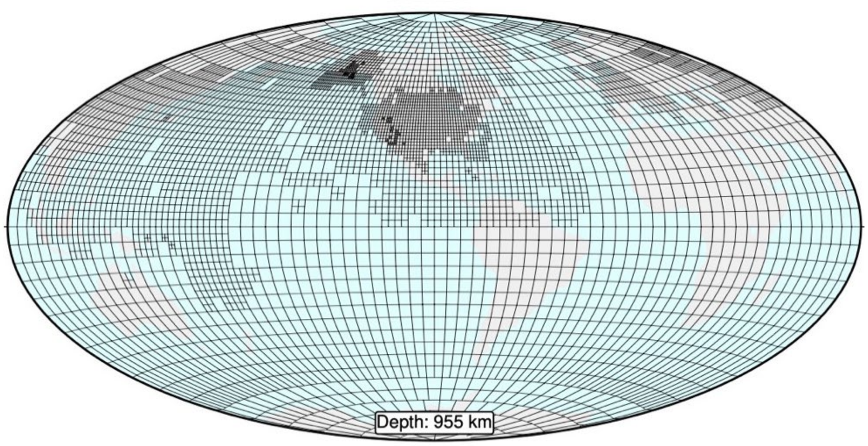
Depth: 955 km

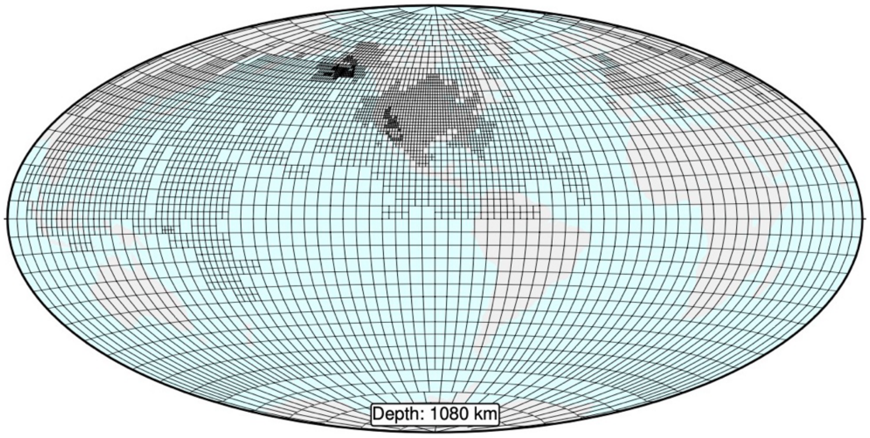
Depth: 1080 km

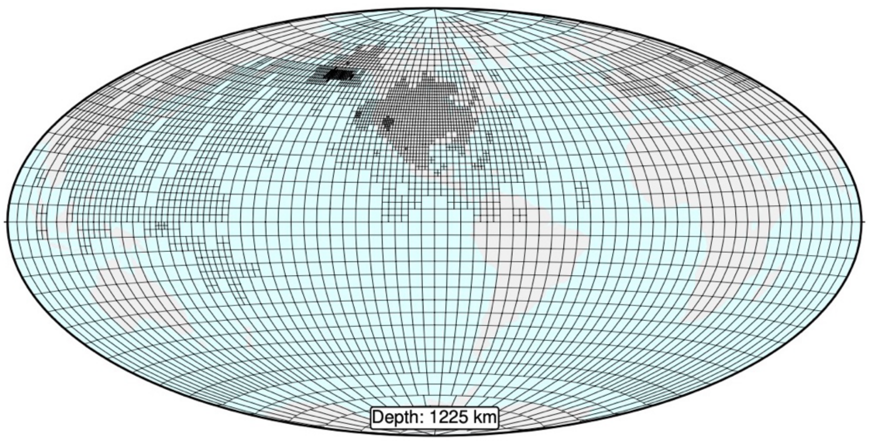
Depth: 1225 km

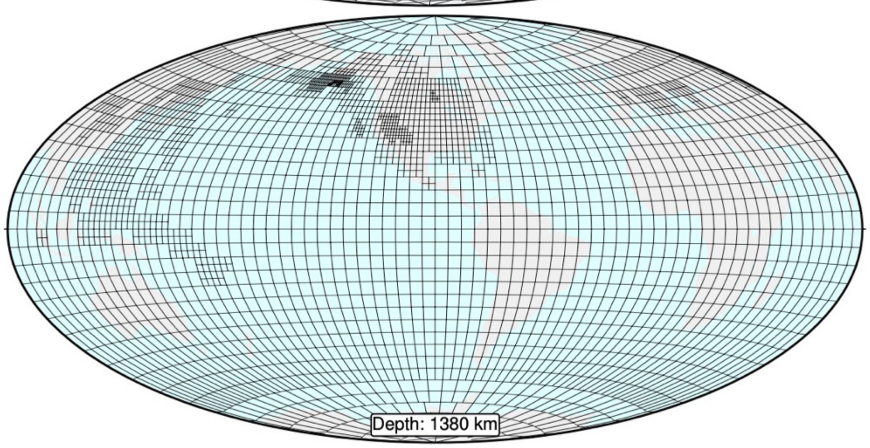
Depth: 1380 km

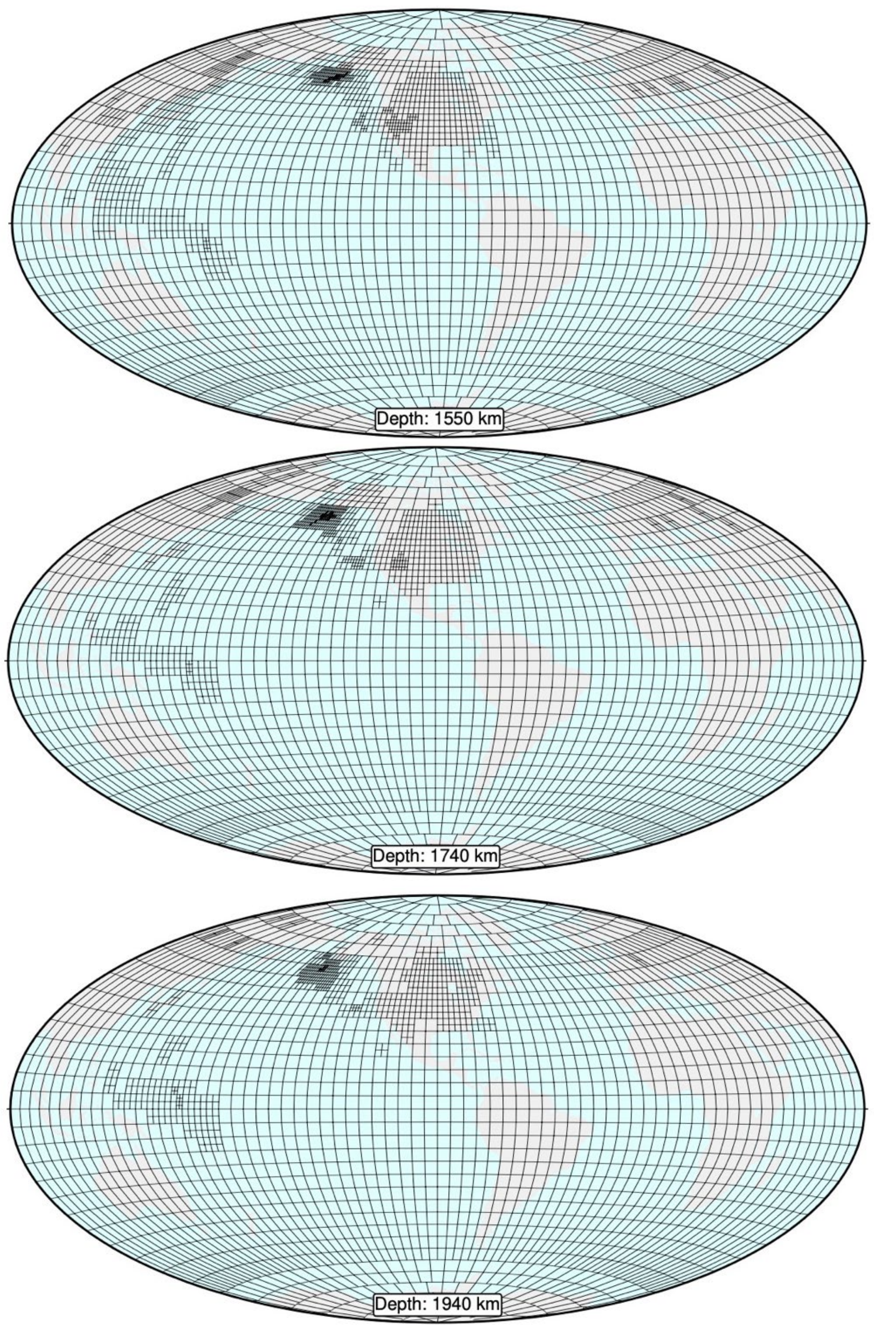
Depth: 1550 km
Depth: 1740 km
Depth: 1940 km

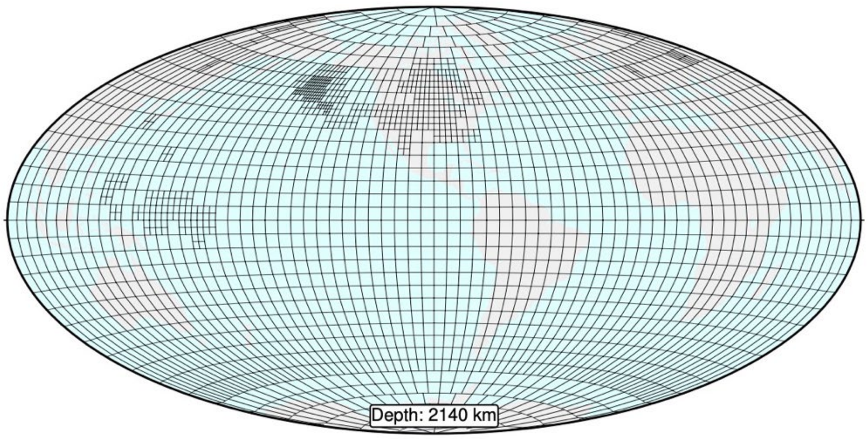
Depth: 2140 km

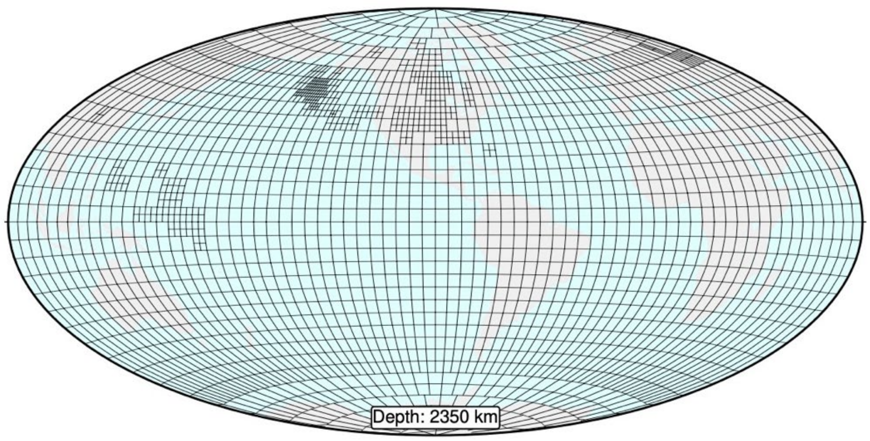
Depth: 2350 km

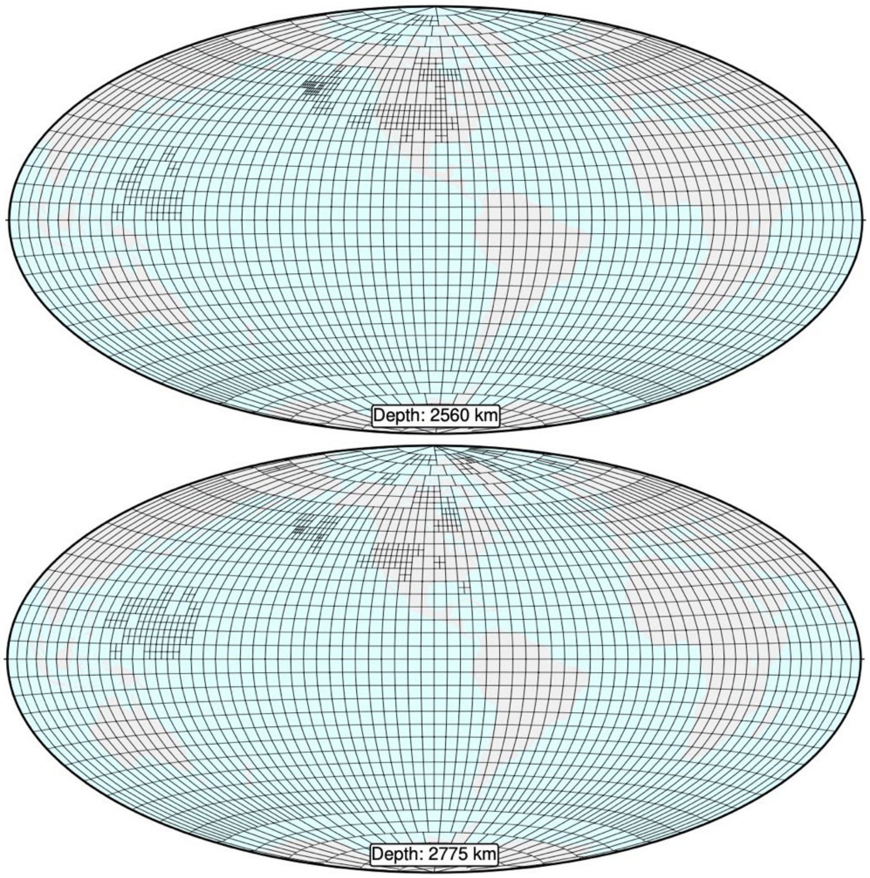

Figure S1: Data adaptive mesh used for the tomographic inversion at each model layer. Bottom of each panel indicates the depth. This mesh was created with the SAVANI software available at https://github.com/rwporritt/savani. Specifically, this depends on hit count adaptive for each voxel. The minimum voxel size is set to 0.3125˚ x 0.3125˚ to a maximum of 5˚ x 5˚ doubling at each step. The thresholds for the global meshing are 5000, 7000, 8000, and 9000 for coarsest mesh to finest mesh. The regional thresholds for North America (longitude 180˚ to 315˚ E and latitude 10˚ to 70˚ N and depth less than 1300 km) are 2000, 3000, 4000, and 5000 hits per voxel.

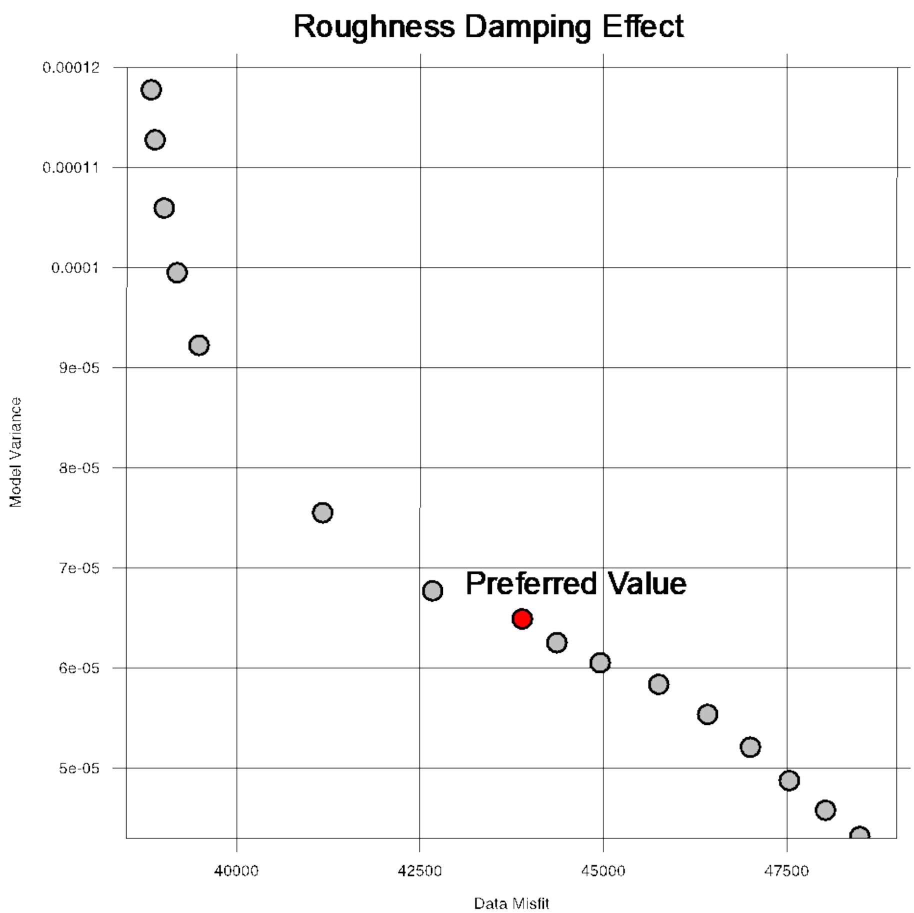

Figure S2: Trade-off curve for tested roughness damping at constant difference damping and norm damping. The red circle is our preferred value for SAVANI-US.

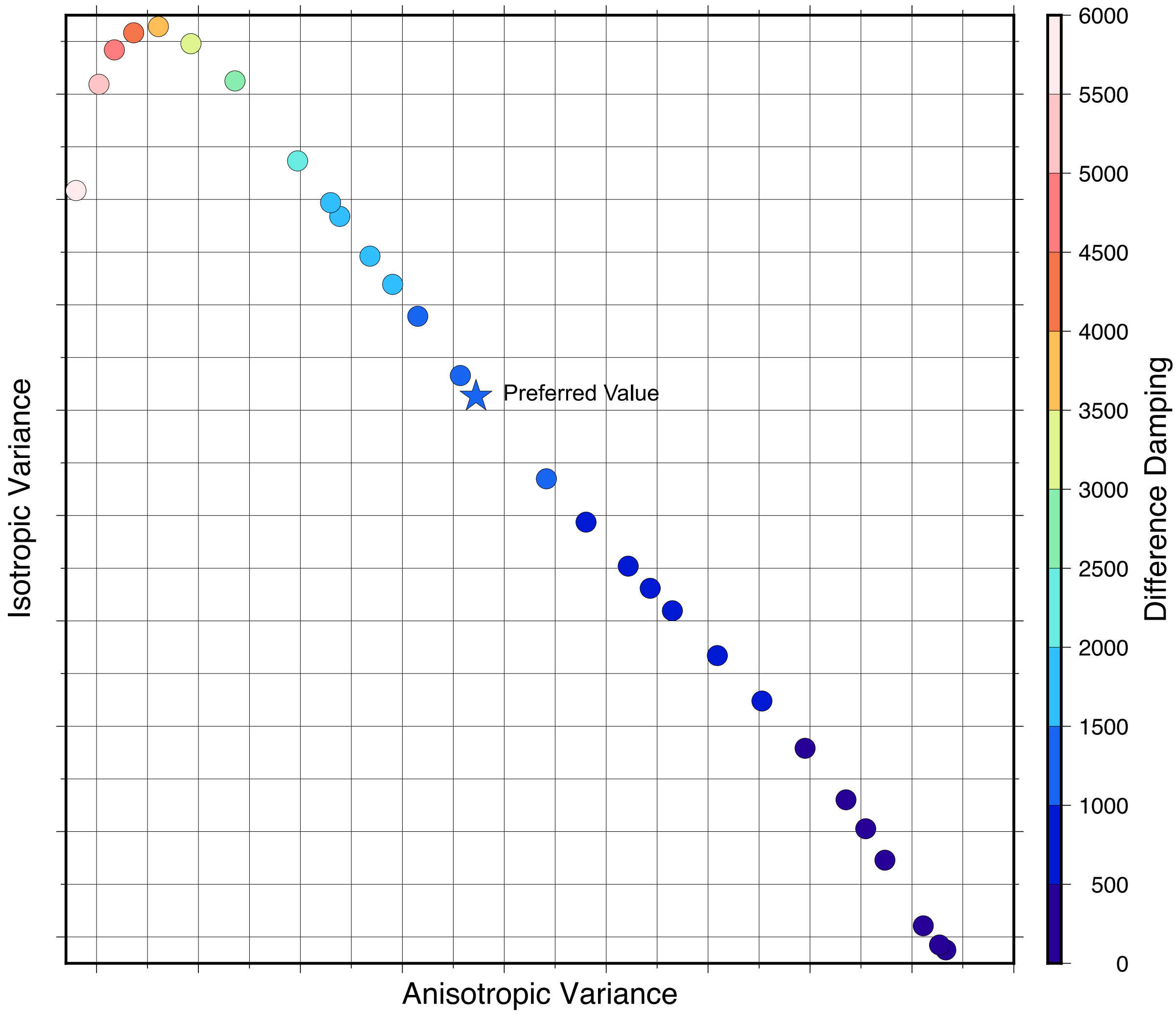

Figure S3: Effect of difference damping parameter on leakage. Most of the explored space is nearly linear and high difference damping values show a local maximum in isotropic variance.

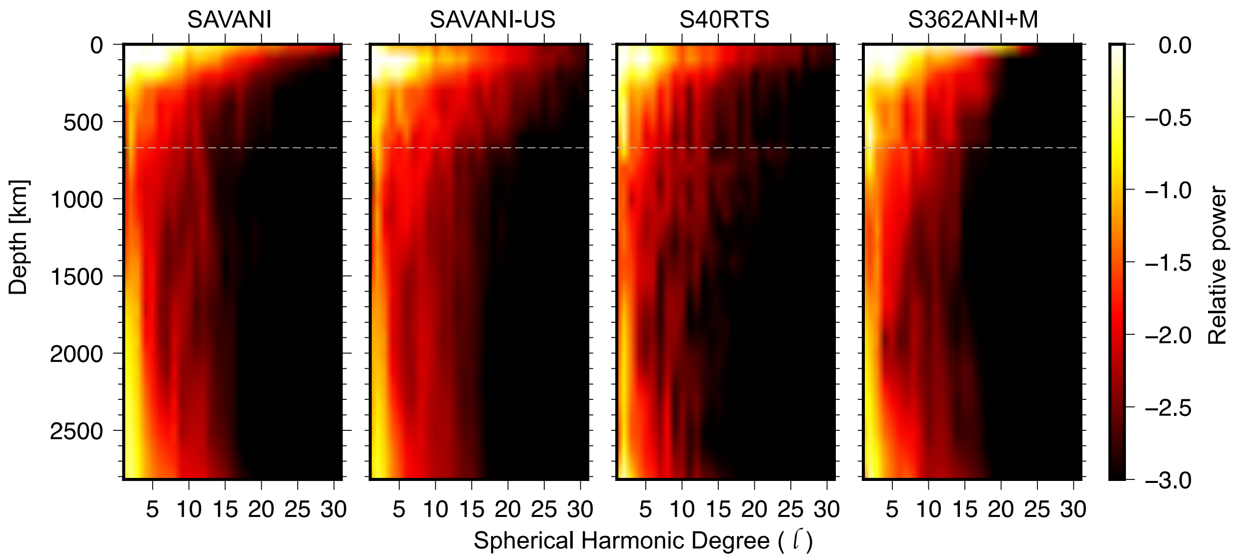

Figure S4: Plot of power spectral density vs. depth and spherical harmonic degree for isotropic velocity models compared in Figure 4. Higher spherical harmonic degree corresponds to shorter wavelength structures. SAVANI is by Auer et al. (2014), SAVANI-US our new model, S40RTS by Ritsema et al. (2011), S362ANI-M by Moulik and Ekstrom (2014).

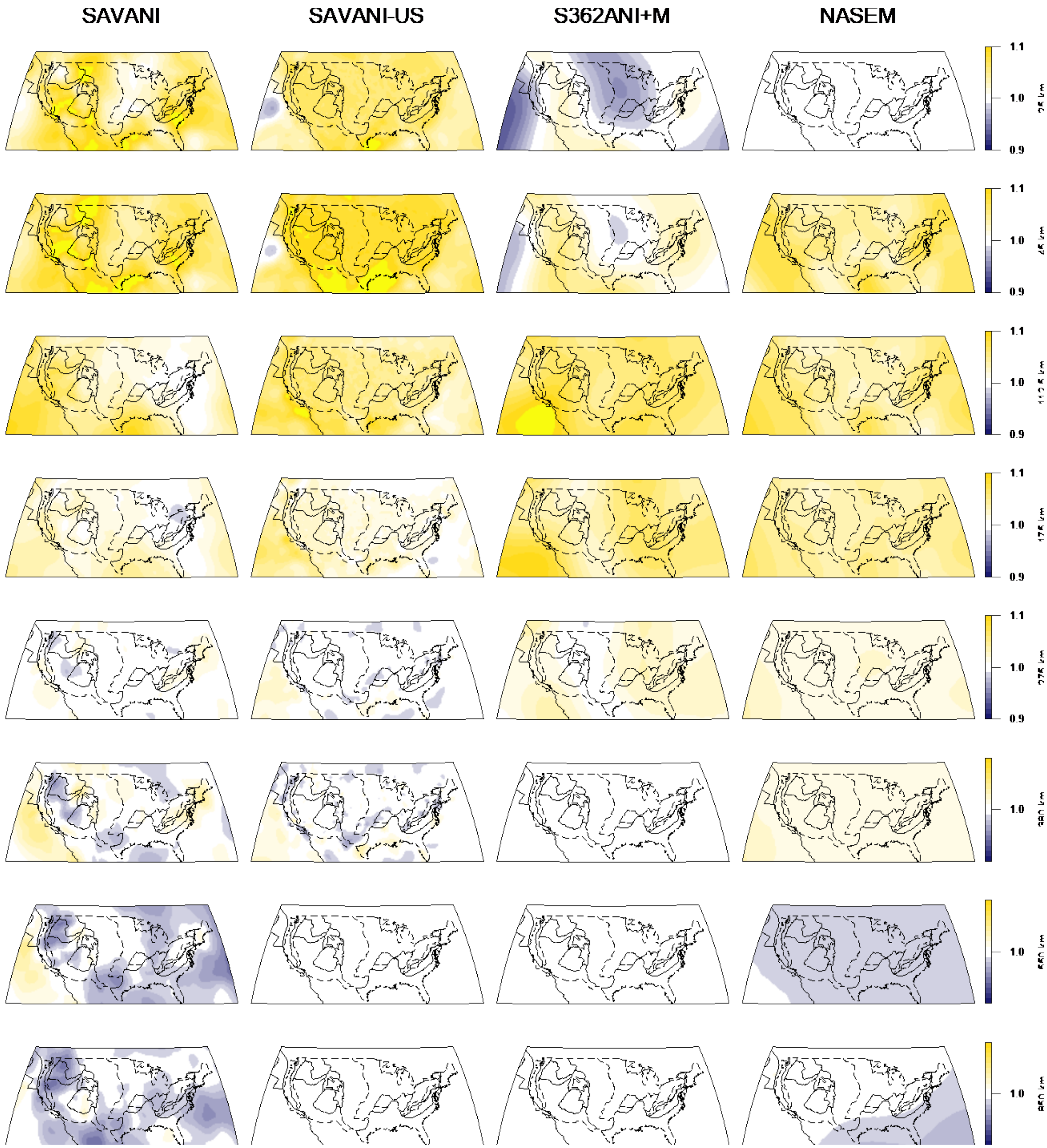

Figure S5: Models of radial anisotropy focused under the contiguous US. Model names on top are the same as per the main paper. NASEM is by Clouzet et al. (2018).

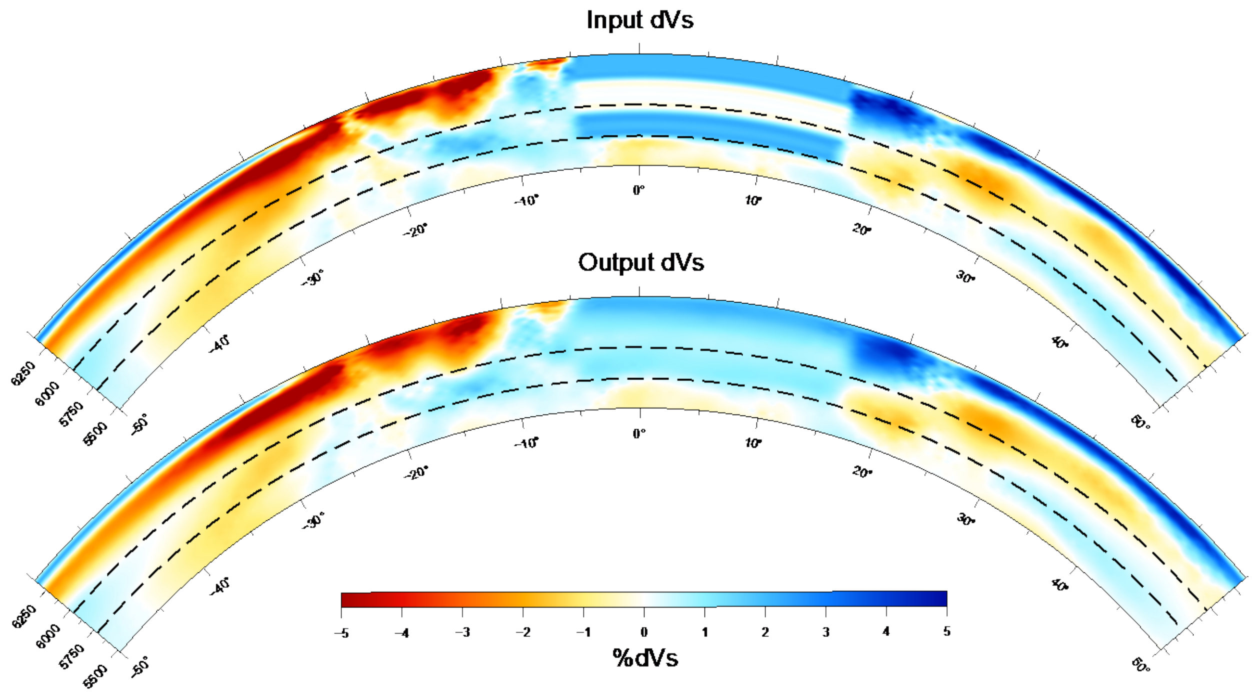

Figure S6: Result of a resolution test with a thick craton in the upper 200 km and a 200 km thick slab in the transition zone. The input model is our best-fit model but with the structure in the central US replaced for the test (top panel). The output shows that the zone of neutral velocity anomaly separating the slab and the craton is poorly resolved and replaced with structure smeared between the slab and the craton.

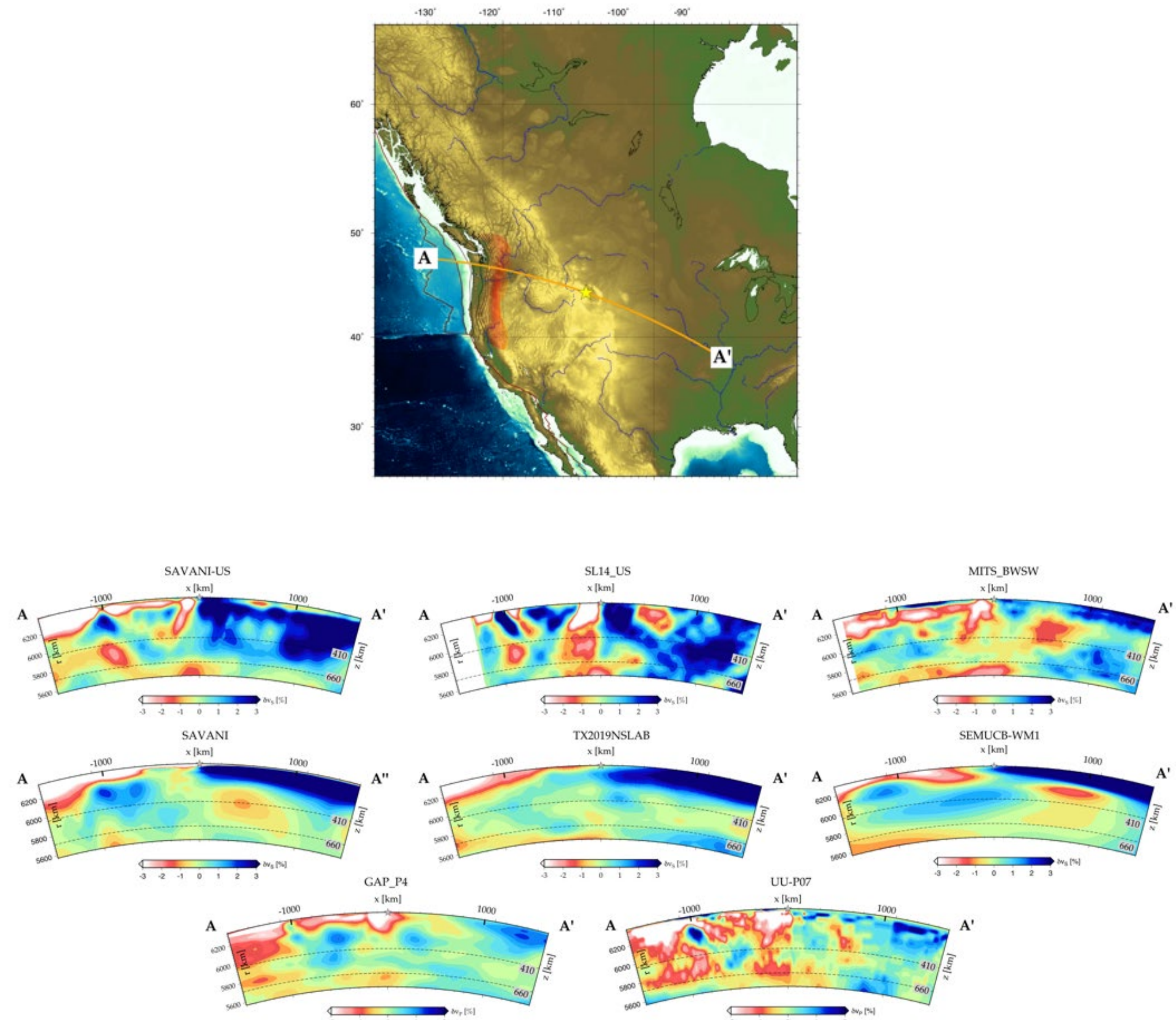

Figure S7: Comparison of seismic tomography models along a profile similar to Figure 7b (A-A’). Models along the top row are focused on the continuous US and use body waves and surface waves in the case of SAVANI-US and MITS_BWSW. Models in the middle row are relatively smooth, global models. Models along the bottom row are P wave only models. MITS_BWSW is by Golos et al. (2018), TX2019 by Lu et al. (2019, version without prescribed slabs), SEMUCB-WM1 by French and Romanowicz (2014), GAP_P4 by Obayashi et al. (2013) and Fukao and Obayashi (2013) and UU-P07 by Amaru (2007) and Hall and Spakman (2015).

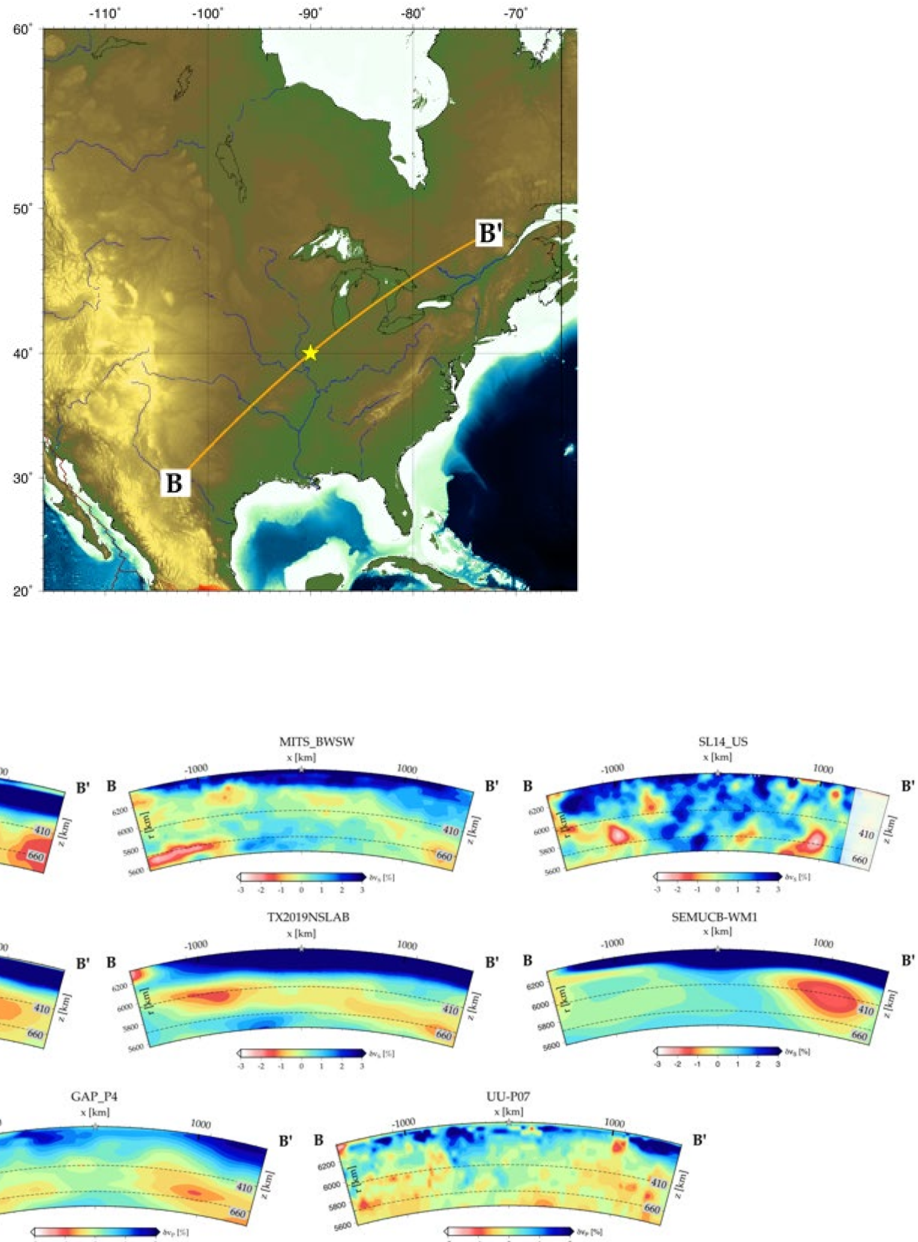

Figure S8: Comparison of velocity models along a profile similar to Figure 7c (B-B'). See caption for S7 for model description.

Additional references cited

Amaru, M.L., 2007, Global travel time tomography with 3-D reference models: Geologica Ultraiectina, 274, 174p.

Fukao Y., M. Obayashi (2013), Subducted slabs stagnant above, penetrating through and trapped below the 660-km discontinuity. J. Geophys. Res., 118, 5920-5938, doi:10.1002/2013JB010466.

Hall, R., and Spakman, W., 2015, Mantle structure and tectonic history of SE Asia: Tectonophysics, 658, 14-45.

Lu, C., Grand, S. P., Lai, H., & Garnero, E. J. (2019). TX2019slab: A new P and S tomography model incorporating subducting slabs. Journal of Geophysical Research: Solid Earth, 124, 11549– 11567. https://doi.org/10.1029/2019JB017448.

Obayashi M., J. Yoshimitsu, G. Nolet, Y. Fukao, H. Shiobara, H. Sugioka, H. Miyamachi, Y. Gao (2013), Finite frequency whole mantle P-wave tomography: Inprovement of subducted slab, Geophys. Res. Lett., 40, 5652-5657, doi:10.1002/2013GL057401.